Damping Region Extension for Digitally Controlled LCL–Type Grid–Connected Inverter with Capacitor–Current Feedback

3 authors, including:

Jinhong Liu
Chongqing University
10 PUBLICATIONS   **38** CITATIONS

Marta Molinas
Norwegian University of Science and Technology
337 PUBLICATIONS   **4,057** CITATIONS

Some of the authors of this publication are also working on these related projects:

Historical review of electrification in marine vessels View project

Optimization-based system-level active harmonic mitigation View project

Damping Region Extension for Digitally Controlled LCL-Type Grid-Connected Inverter with Capacitor-Current Feedback

Jinhong Liu [1, 2*], Lin Zhou[1], Marta Molinas[2]

[1]College of Electrical Engineering, Chong Qing University, Chong Qing 400044, China
[2]Department of Engineering Cybernetics, Norwegian University of Science and Technology, Trondheim 7491, Norway
*jinhongliu.felix@gmail.com

Abstract: This paper investigates the extent to which the damping region of a digitally controlled LCL-type grid connected inverter is influenced by the ratio between sampling and switching frequencies, the grid impedance variation and changes in the LCL filter. Based on this analysis, an improved capacitor-current feedback is proposed to preserve stability by extending the damping region under the critical conditions identified. The attention is focused on the case when the system switching frequency is higher than one-half of the system sampling frequency, which is not covered in the existing literature. In this case, the undamped region is obviously expanded and a conventional capacitor-current feedback will not provide sufficient damping region. An improved capacitor-current feedback active damping method is proposed to increase the system critical frequency greatly and to obtain a wider damping region for all possible LCL resonances. With a reasonable parameter design, the extended system damping region is able to cover almost all possible resonance frequencies even when the switching frequency is the same as sampling frequency. A high robustness to grid-impedance variation is achieved in the system as a result of this improved feedback control. The effectiveness of the theoretical analysis and proposed method are verified by the experimental results.

1. Introduction

With the development of renewable energy technology, as the interface between a renewable energy generation system and the power grid, inverters have been attracting increasing attention [1]-[14]. To inject power into the grid with low distortion, LCL filter is often used in all of the medium-high power grid-connected inverters with low switching frequency because its unique advantages compared with the L filter [15]. However, the stability of the inverter system may be influenced by the inherent resonance characteristics of the LCL filter [3]. In order to dampen the LCL resonance without increasing the power loss and undermining the harmonic attenuation ability of LCL filter, the active damping method is usually adopted in high power level inverter [1]-[9]. Among the various active damping solutions, the capacitor-current feedback active damping approach is one of the most widely used methods for its effectiveness and simple implementation [16]. However, when a digital control system is employed, the active damping performance may be affected by the effects of digital time delay.

Generally, for a digitally controlled system, the digital time delay in the system mainly consists of computation and PWM delay. The computation delay is the time required for translating the external sampled signal into a PWM reference signal and it will change as the duty ratio update mode varies [17].

The PWM delay is caused by the zero-order-hold (ZOH) effect, which keeps the PWM reference signal before it is compared to the triangular carrier and it can be seemed as half sampling period length [8]. With the wide application of the digital control system in the LCL-type grid-connected inverter with capacitor-current feedback, the system stability of a digitally controlled LCL-type grid-connected inverter with this feedback has been studied in many publications. Orellana and Griñó. [18] investigated capacitor-current feedback active damping in the *s*-domain and the *z*-domain, and found that a one-step computation delay might aggravate the system instability, but no method to enhance the system stability was provided. To stabilize the system with digital time delay, Miskovic *et al.* [19] used a Luenberger observer as a sensor replacement and state predictor to alleviate the impact of a one-step computational delay, which greatly improved the active damping capability. However, the parameters of the state observer are sensitive to the system parameters and thus the system may become unstable as the system parameters changes. Chen *et al*. [20] proposed a time delay method based on the area equalization concept. This method is simple and effective, but it can only compensate a system with a time delay lower than a half sampling period. Pan *et al*. [8] shifted the capacitor-current sampling instant towards the reference update time of PWM to reduce the digital time delay. Nevertheless, aliasing might occur if the capacitor-current samping time is not properly located.

Moreover, in addition to the method of time delay compensation that is adopted to ensure the stability of the digitally controlled LCL-type grid-connected inverter with capacitor-current feedback, the method to guarantee the stability of the system with time delay by extending system damping region has also been explored in many publications. In [3], [5], [8]-[10], and [21]-[23], one-sixth sampling frequency (f_s/6) is identified as the critical frequency for stabilizing a digitally controlled LCL-type grid-connected inverter. Bao *et al.* [3] showed that the design of the system controller parameters and the damping coefficient are significantly determined by the system critical frequency. Parker *et al*. [21] found that when the system resonance frequency is higher than f_s/6, active damping is not required to stabilize the system. However, Li *et al*. [10] found that even if the system is stable when the resonance frequency is higher than f_s/6, the active damping method is also necessary because the potential for resonance shifting makes the system more susceptible to instability. Subsequently, two different damping region extension methods were proposed in [10] and [23] to increase the system critical frequency to $0.25f_s$ and f_s/3, respectively. However, the system in [10] and [23] were discussed and analysed under the case of the system switching frequency is equal to half of the system sampling frequency. Considering the system resonance frequency should be chosen in a range between ten times the line frequency (f_0) and one half of the switching frequency [15], which indicates the system possible resonance frequency range is ($50f_0$, $0.25f_s$) when the system switching frequency is equal

to half of the system sampling frequency, the upper limit of the damping region are extended to around $0.25f_s$ in previous works, such as the upper limit of the damping region in [10] and [23] are $0.25f_s$ and $f_s/3$, respectively. However, the ratio between sampling frequency (f_s) and switching frequency (f_{sw}) varies with the sampling mode of the system (For example, the ratio between f_s and f_{sw} is 2 in natural sampling, and it will change to 1 in the symmetric regular sampling). Hence, the extended system damping region in [10] and [23] may not be sufficiently high to cover all possible system resonance frequencies when the sampling frequency is the same as the switching frequency which the system possible resonance frequency range is $(50f_0, 0.5f_s)$ in this case, and thus the system becomes vulnerable to work outside the damping region which may leads to instability [10].

This paper focuses on addressing the stability problem of digitally controlled grid-inverter system in different sampling modes meaning that the system switching frequency may be larger than one-half of the system sampling frequency, by proposing an improved capacitor-current feedback active damping method. In Section 2, the equivalent s-domain and z-domain models of the digitally controlled LCL-type grid-connected inverter with capacitor-current feedback are derived. Then, based on the obtained model, the effects of damping region on system are comprehensively investigated in Section 3. In Section 4, an improved capacitor-current feedback active damping method for widening the system damping region is introduced, and the stability of the improved system is discussed. Experimental results are presented in Section 5 to validate the proposed method. Section 6 concludes the paper.

2. Modeling the grid-connected inverter

2.1. System Description

The typical digitally controlled three-phase grid-connected voltage source inverter system with an LCL filter is shown in Fig. 1. The LCL filter circuit consists of an inverter-side inductor L_1, a capacitor C_f and a grid-side inductor L_2. The grid inductance L_g comprises the line inductance and the transformer inductance. The parasitic resistances associated with inductors and capacitors are ignored to represent the worst case in the analysis.

According to Fig. 1a, the transfer functions from the inverter-side voltage to the grid-side current and to the capacitor current can be expressed in (1) and (2), respectively, with $\omega_r = \sqrt{(L_1 + L_t)/L_1 L_t C_f}$, $\omega_1 = \sqrt{1/L_t C_f}$ and $L_t = L_2 + L_g$.

$$G_{ig}(s) = \frac{i_g(s)}{u_i(s)} = \frac{\omega_1^2}{sL_1(s^2 + \omega_r^2)} \tag{1}$$
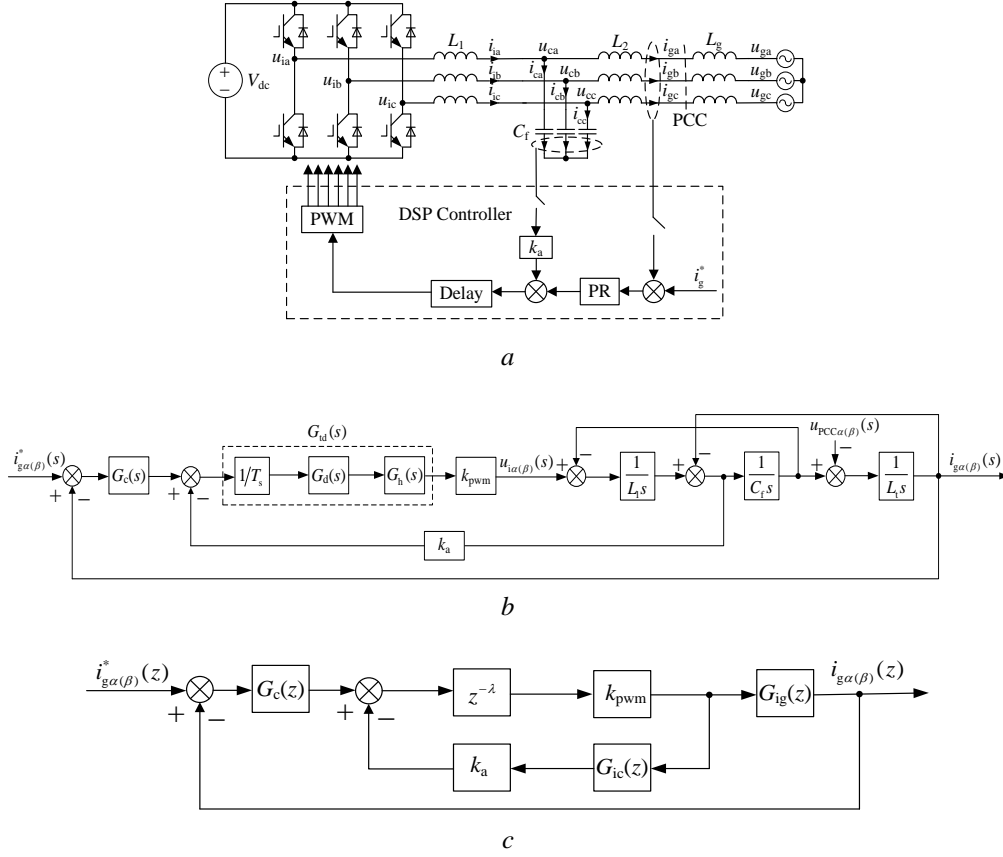
Fig. 1. *Digitally controlled LCL-type three-phase grid-connected inverter with capacitor-current feedback active damping*
a Power Circuit
b Control block diagram in the *s*-domain
c Control block diagram in the *z*-domain

$$G_{ic}(s) = \frac{i_c(s)}{u_i(s)} = \frac{s}{L_1(s^2 + \omega_r^2)} \tag{2}$$

2.2. Digital control loop

To implement an independent control in the control loop without using a decoupling module, the scheme of the digital control loop for the grid-side current i_g is developed in a stationary frame, as shown in Fig. 1*b*. $G_c(s)$ is the current controller, and a proportion-resonant (PR) controller is provided in (3), where k_p is the proportional gain, k_r is the resonant gain, ω_i is the resonant cutoff angular frequency, and ω_0 is the fundamental angular frequency.

$$G_c(s) = k_p + \frac{2k_r\omega_i s}{s^2 + 2\omega_i s + \omega_0^2} \tag{3}$$

As mentioned in [5], the processes of sampling, computation and signal update lead to a time delay in a digital system that is expressed in terms of the sampling period T_s as λT_s ($0 \le \lambda \le 1$), and can be modeled

in the *s*-domain as $G_d(s) = e^{-s\lambda T_s}$ and $\lambda = 1$ for the synchronous sampling case [8].

After obtaining the PWM reference signal, the updated PWM reference signal is held and compared to the triangular carrier to generate the duty cycle, and this process can be expressed as ZOH in the *s*-domain [20].

$$G_h(s) = \frac{1 - e^{-sT_s}}{s} \approx T_s e^{-0.5sT_s} \tag{4}$$

Therefore, the total time delay in the digital control loop is $(\lambda+0.5)T_s$ and can be expressed in the *s*-domain as

$$G_{td}(s) = e^{-s(\lambda+0.5)T_s} \tag{5}$$

Moreover, k_{pwm} represents the gain of the PWM inverter, and the sampler is represented by $1/T_s$ [8].

Fig. 1*c* shows the *z*-domain control model, where $G_{ig}(z)$ and $G_{ic}(z)$ are derived by applying a modified *Z*-transform to (1) and (2) with ZOH [3]

$$G_{ig}(z) = \frac{k_{pwm}}{L_1 + L_t} \left[\frac{B\omega_r T_s (mz + 1 - m) - A(z-1)^2}{B\omega_r z(z-1)} \right] \tag{6}$$

$$G_{ic}(z) = \frac{Ak_{pwm}(z-1)}{B\omega_r L_1 z} \tag{7}$$

where $A = z\sin(m\omega_r T_s) + \sin[(1-m)\omega_r T_s]$, $B = z^2 - 2z\cos(\omega_r T_s) + 1$ and $m = 1 - \lambda \ (0 \le m \le 1)$. Therefore, the open-loop transfer function of the system can be obtained as

$$T(z) = \frac{G_c(z) L_1 k_{pwm} [B\omega_r T_s (mz + 1 - m) - A(z-1)^2]}{(L_1 + L_t)(z-1)[B\omega_r L_1 z + Ak_{pwm}k_a(z-1)]} \tag{8}$$

where $G_c(z) = k_p + \dfrac{2k_r\omega_i T_s(z-1)}{z^2 + (\omega_0^2 T_s^2 + 2\omega_i T_s - 2)z - 2\omega_i T_s + 1}$, and $m=0$ and $m=1$ represent the situations of one-step delay and no computation delay, respectively.

3. Damping region effects on system

Because the existence of digital time delay, the system critical frequency is decreased from $f_s/2$ to $f_s/6$, which means the range of damping region of LCL-type grid-connected inverter with capacitor-current feedback is reduced from $(0, f_s/2)$ to $(0, f_s/6)$ [8]. Considering the possible distribution of system resonance frequency is $(50f_0, f_s/2)$, the system may work in a large region of $(f_s/6, f_s/2)$, which is not covered by the damping region. Therefore, based on the model obtained in Section 2, the effects of damping region on system are investigated in this section.

Table 1 Main Parameters of the Grid-Connected Inverter

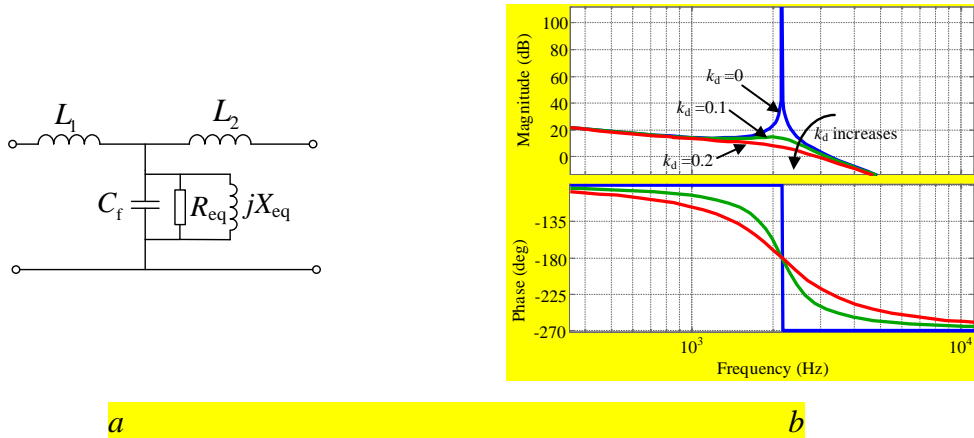| Parameters	Case I	Case II	Case III
DC-side voltage V_{dc}		720 V	
Grid-side voltage V_g		220 V	
Fundamental frequency f_0		50 Hz	
Switching frequency f_{sw}		10 kHz	
Sampling frequency f_s		20 kHz	
Inverter-side inductor L_1		4 mH	
Filter capacitor C_f		2.5 μF	
Grid-side inductor L_2		0.4 mH	
Grid-side inductor L_g	2 mH	2 mH	0.02 mH
Damping coefficient k_d	0.09	0.12	0.18

F

a

b

Fig. 2. Equivalent circuit and Bode diagram
a. Equivalent circuit of the virtual impedance
b. Bode diagram of $T(z)$ with $G_c(z)=1$

3.1. Impacts of resonance damping

Referring to Fig. 1*b*, through a series of equivalent transformations, the active damping loop can be equivalent to a virtual impedance $Z_{eq}(j\omega)$ in parallel with the filter capacitor, as shown in Fig. 2*a* and it can be expressed as [8]

$$Z_{eq}(j\omega)=R_{eq}(\omega)//jX_{eq}(\omega) \tag{9}$$

6

where $R_{\mathrm{d}} = L_1 / k_{\mathrm{pwm}} k_{\mathrm{a}} C_{\mathrm{f}}$, $R_{\mathrm{eq}}(\omega) = R_{\mathrm{d}} \dfrac{1}{\cos(\lambda + 0.5)\omega T_{\mathrm{s}}}$, $X_{\mathrm{eq}}(\omega) = R_{\mathrm{d}} \dfrac{1}{\sin(\lambda + 0.5)\omega T_{\mathrm{s}}}$.

In (9), R_{eq} determines the damping effect of the active damping loop, and the active damping coefficient k_{d} directly affects the value of R_{eq}.

Fig. 2*b* show the Bode diagram of loop gain $T(z)$ with the parameters listed in Table 1 when $G_{\mathrm{c}}(z)=1$. As seen, when the active damping coefficient k_{d} is 0, the active damping has no contribute to the resonance damping and thus the magnitude has an infinite resonance gain at system resonance point.

Table 2 Key Features and Stability Requirements of Digitally Controlled Inverter with Capacitor-Current-Feedback

|	Key Features	Stability Requirements
Case I	$f_r < f_s/6$, $k_a < k_{ac}$ and no open-loop unstable pole	$MD_r < 0$
Case II	$f_r < f_s/6$, $k_a > k_{ac}$ and a pair of open-loop unstable poles	$MD_r < 0$ and $MD_c > 0$
Case III	$f_r > f_s/6$, $k_a > 0$ and a pair of open-loop unstable poles	$MD_r > 0$ and $MD_c < 0$

3.2. Robustness against grid impedance variation

Table 2 lists the key features and stability requirements of digitally controlled grid-connected inverter with capacitor-current feedback, where $k_{ac} = \dfrac{\omega_r L_1 (2\cos\omega_r T_s - 1)}{k_{pwm}\sin\omega_r T_s}$, $MD_r = 20\lg\dfrac{k_p L_1}{k_a(L_1 + L_2 + L_g)}$,

$MD_c = 20\lg\left|\dfrac{k_p(\sin\omega_r T_s + \omega_r T_s(1 - 2\cos\omega_r T_s))}{(L_1 + L_2 + L_g)(k_a k_{pwm}\sin\omega_r T_s + \omega_r L_1(1 - 2\cos\omega_r T_s))}\right|$. Then with the parameters listed in Table 1, Fig.

3a-3c shows the curves of MD_r and MD_c varies with the grid inductance L_g, where the grid inductance L_g varies from 0 to 10% PU that corresponds to a short-cut ratio of 10, and the system resonance frequency f_r is equal to $f_s/6$ when $L_g = 1.18$ mH. As seen, when the system initial work in the *Case* I and *Case* II with certain parameters, which the system resonance frequency within the damping region, the system can be stable as the grid inductance varies in (1.18 mH, 2 mH) and becomes unstable when L_g below 1.18 mH that corresponds to *Case* III. When system original work in *Case* III, it can be seen from Fig. 3c that, in condition of certain parameters of k_p and k_a, system remains stable only in a small range of L_g in *Case* III, which is (0, 0.25 mH) in the case shown in Fig. 3c.
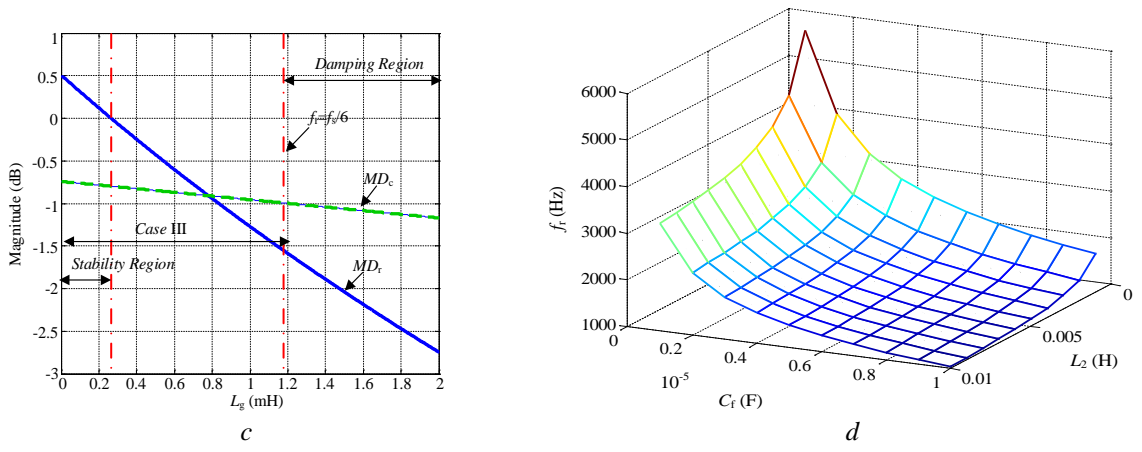

a

b
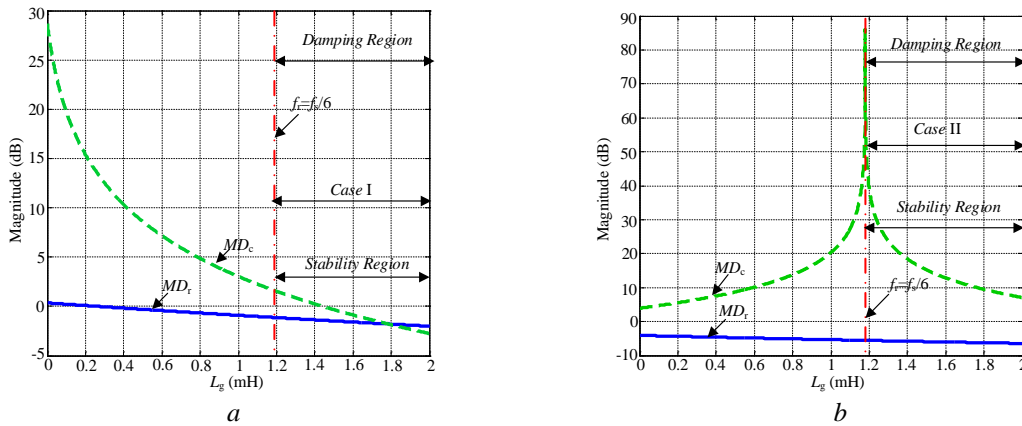
Fig. 3. *Curves of MD_r, MD_c and f_r*
a Curves of MD_r and MD_c as L_g varies when the system initial work in the *Case* I
b Curves of MD_r and MD_c as L_g varies when the system initial work in the *Case* II
c Curves of MD_r and MD_c as L_g varies when the system initial work in the *Case* III
d Curves of f_r with C_f and L_2 varies

The above analysis identifies that the system has a high robustness against grid impedance variation when the system initially works in the system damping region. In practical situations, because the variation of grid impedance due to the change of load, the variation of resonance frequency f_r may cause the system to work from one case to another. Meanwhile, since there is no high-frequency unstable poles, the output current of the inverter in *Case* I has better quality than the systems in *Case* II and *Case* III. Therefore, if the system critical frequency can be higher than most of possible resonance frequencies or even the allowed maximum system resonance frequency that can be derived by the LCL design criterion [15], the system can obtain a large damping region that make system always work in *Case* I, and thus the system can be more stable.

3.3. Parameters of LCL filter

Based on the above analysis, to better ensure high stability and robustness of the digitally controlled grid-connected inverter system, it is best to choose a system resonance frequency (f_r) that is lower than the system critical frequency ($f_s/6$). Fig. 3d shows that curves of resonance frequency f_r as C_f and L_2 varies, where L_g=0 H, L_1 is chosen as 4 mH to obtain a low harmonic current below the IEEE-519 limitations and the ranges of C_f and L_2 are also obtained according to the design criteria of LCL filter [15]. As seen, to make system resonance frequency lower than system critical frequency ($f_s/6$), at least one large value is required between C_f and L_2. However, a larger inductance and capacitance in the LCL filter will cause an increase of filter volume and thus increased costs [15].

Therefore, it can be concluded from the above analysis that, in order to improve the robustness of the system while maintaining a good quality of output current, a higher critical frequency is desirable. In doing

9

so, according to the previous discussion, the system stability requirements will become much easier to satisfy while achieving a higher robustness against grid impedance variation at the same time.
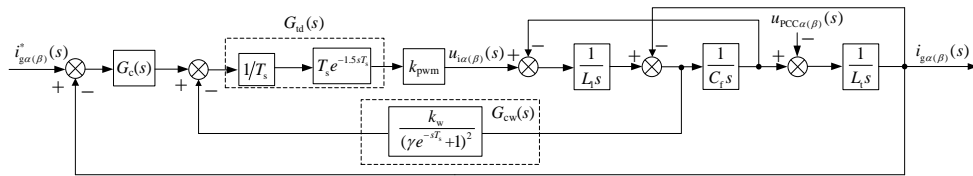
4. Grid-Connected inverter with improved capacitor-current feedback active damping

According to the analysis in Section 3, a higher system critical frequency is essential to ensure system work in damping region that can obtain high stability and robustness in a digitally controlled grid-connected inverter with capacitor-current feedback. Considering the method in previous work may not sufficient to obtain a high quality output current and the system is vulnerable to become unstable due to the system resonance frequency shifting when the sampling frequency is equal to the switching frequency, an improved capacitor-current feedback method is required to the further increase of the system critical frequency. Therefore, considering the increase of critical frequency in the case of the system switching frequency is higher than half of the system sampling frequency, and complexity of system design, a new feedback link of capacitor-current ($G_{cw}(z)$) is proposed based on the recursive infinite impulse response (IIR) digital filter [24], to extend the system critical frequency which is directly related to the system damping region.

$$G_{cw}(z) = \frac{k_w}{(1+\gamma z^{-1})^2} \tag{10}$$

Fig. 4a shows the grid-connected inverter system control model with improved capacitor-current feedback in the s-domain, where $G_{cw}(s)$ is the s-domain transfer function of (10) and can be expressed as

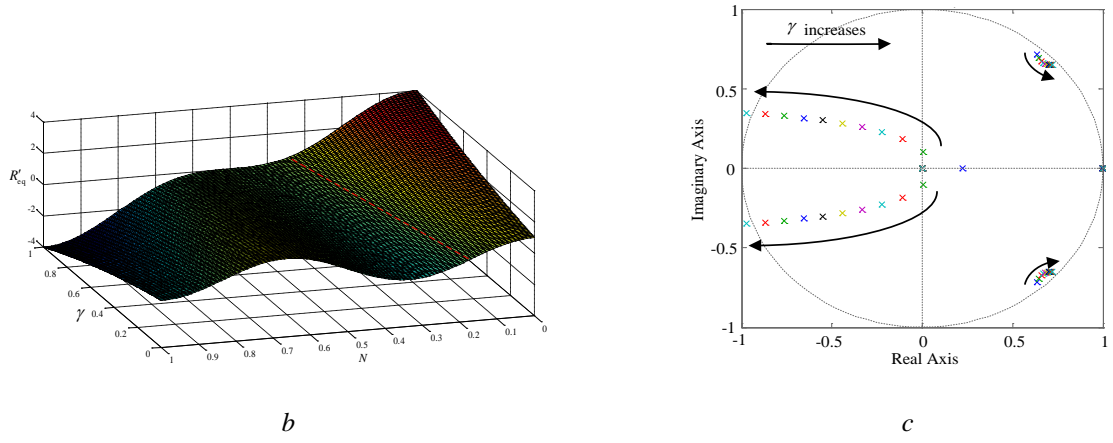$$G_{cw}(s) = \frac{k_w}{(\gamma e^{-sT_s}+1)^2} \tag{11}$$

a

b

c

Fig. 4. *The inverter with improved capacitor-current feedback active damping*
a Control block diagram in the *s*-domain
b Relationships between N, γ and R'_{eq}
c Poles maps of $T'(z)$ with γ varies

According to Fig. 4*a*, the equivalent impedance $Z'_{eq}(s)$ in improved system can be derived as

$$Z'_{eq}(s) = \frac{L_1 T_s}{k_{pwm} C_f G_{td}(s) G_{cw}(s)} = R'_d (\gamma e^{-sT_s} + 1)^2 e^{1.5sT_s} \tag{12}$$

where $R'_d = \dfrac{L_1}{k_{pwm} k_w C_f}$. Substituting $s = j\omega$ into (12), then yields

$$Z'_{eq}(j\omega) = R'_{eq}(\omega)//jX'_{eq}(\omega) \tag{13}$$

where

$$\begin{cases} R'_{eq}(\omega) = \cos 1.5\omega T_s + (\gamma^2 + 2\gamma)\cos(0.5\omega T_s) \\ X'_{eq}(\omega) = \sin 1.5\omega T_s + (-\gamma^2 + 2\gamma)\sin(0.5\omega T_s) \end{cases} \tag{14}$$

From (14), with defining the system resonance frequency f_r as N ($0<N<1$) times the sampling frequency f_s, the relationships between the N, γ and R'_{eq} can be shown in Fig. 4*b*. As seen, the range of $R'_{eq} > 0$ increases with increasing of γ, which indicates the system damping region will extend as γ increases. However, apart from considering the extension of the damping region, the system stability also should be considered in the design of the improved active damping loop.

4.1. Parameters design of the improved capacitor-current feedback

Based on Fig. 4*a*, through an equivalent *z*-domain transformation , the open-loop transfer function of the system with improved capacitor-current feedback active damping in *z*-domain can be derived as

$$T'(z) = \frac{G_c(z)L_1 k_{pwm}[B\omega_r T_s - (z-1)^2 \sin \omega_r T_s]}{(L_1 + L_t)(z-1)[B\omega_r L_1 z + k_{pwm}(z-1)G_{cw}(z)\sin \omega_r T_s]} \tag{15}$$

11

Based on (15), the open-loop poles maps with $G_c(z)=1$ for γ variation from 0 to 1 is illustrated in Fig. 4c. As seen, with γ increasing from 0 to 1, the poles gradually approach the unit circle and finally go outside the unit circle when γ is increased to 1. Therefore, considering the extension of the damping region and to avoid the open-loop unstable poles in the open-loop system, $\gamma=0.98$ is chosen. Then, by solving the equation of R'_{eq} in (14), the critical frequency of the system with an improved active damping loop can be obtained as $0.45f_s$.

Moreover, in (15), when $G_c(z)=1$, except for the pole of $z=1$, the other poles are related to the active damping loop, then extracting the partial factor from the denominator of $T'(z)$:

$$Den'(z) = z(z+0.98)^2(z^2 - 2\cos(\omega_r T_s)z + 1) + k_{pwm}k_w\sin(\omega_r T_s)(z^3 - z^2)/\omega_r L_1 \tag{16}$$

According to Jury's criterion, to avoid having poles outside the unit circle, following situation must be satisfied:

$$\begin{cases} \left|1 - a_1^2\right| > \left|a_2 - a_1 a_4\right| \\ \left|(1 - a_1^2)^2 - (a_2 - a_1 a_4)^2\right| > \left|(1 - a_1^2)(a_3 - a_1 a_3) - (a_4 - a_1 a_2)(a_2 - a_1 a_4)\right| \end{cases} \tag{17}$$

where $\delta = k_{pwm}k_w\sin\omega_r T_s / \omega_r L_1$, $a_1=0.9604$, $a_2 = 1.96 - 1.9208\cos(\omega_r T_s) - \delta$, $a_3 = 1.9604 - 3.92\cos(\omega_r T_s) + \delta$, $a_4 = 1.96 - 2\cos(\omega_r T_s)$. Thus, when the resonance angular frequency is determined, the stability range of k_w can be obtained by (17).

Furthermore, for the case of unstable poles exists, according to the Nyquist stability criterion, the system can be stable only when the value of $N_+ - N_-$ is equal to half of the number of unstable poles. Therefore, it is necessary to investigate the $-180°$ crossing of $T'(z)$. From (15), with $G_c(z)$ simplified as k_p and z substituted by $e^{j\omega T_s}$, the phase of $T'(z)$ can be derived as

$$\angle T'(j\omega) = \text{actan}\frac{b_1 d_2 - b_2 d_1}{b_1 d_1 + b_2 d_2} - \pi \tag{18}$$

where b_1, b_2, d_1 and d_2 are listed in the Appendix due to the limitation of space.

From (18), the relationships between the phase of $T'(z)$, N and k_w in two cases: $f_r < 0.45f_s$ and $f_r > 0.45f_s$, are illustrated in Fig. 5. It can be seen from Fig. 5a that, when $0 < k_w < k_{wc}$ (where k_{wc} is the maximum value of k_w that can ensure the open-loop poles are inside the unit circle and can be obtained by (17)), there exist three $-180°$ crossing points in the frequency range, with the first one located at the LCL resonance frequency, the second one located at the left side of $0.45f_s$ and the third one located at $0.5f_s$. If $k_w > k_{wc}$, only two $-180°$ crossing points are in the frequency range, with one of the crossing points
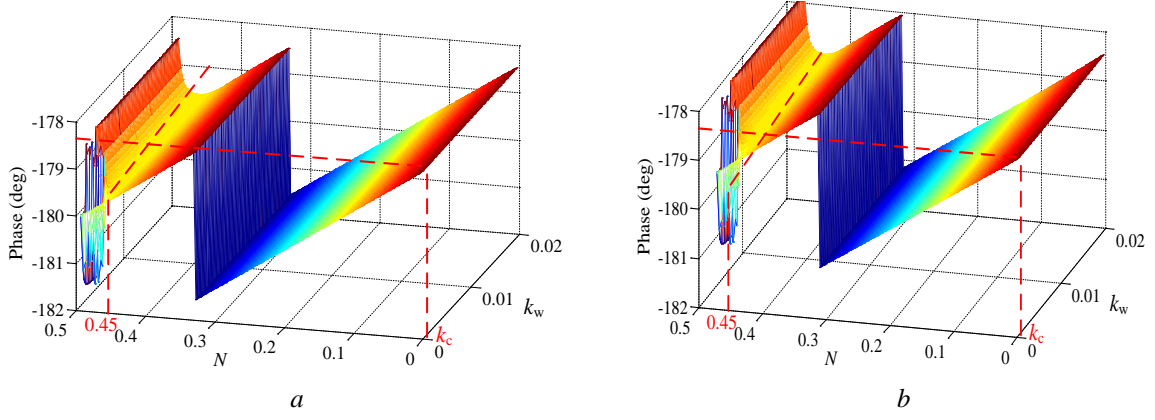
Fig. 5. *Relationships between the phase of* $T'(z)$, *N and* k_w
a When $f_r < 0.45 f_s$
b When $f_r > 0.45 f_s$

located at the LCL resonance frequency and the other one located at $0.5f_s$. Note that, similar to the case of $f_r < 0.45 f_s$, there also exists a boundary value of k_w in the case of $f_r > 0.45 f_s$, which is denoted by k_c in Fig. 5*b* and can be obtained by solving (18). When $0 < k_w < k_c$, there are four $-180°$ crossing points in the system, with one point located at $f_s/6$, two points located between the $0.45 f_s$ and $0.5f_s$, and the last point located at $0.5f_s$. Moreover, when $k_w > k_c$, there are two $-180°$ crossing point in the system, with one located at $f_s/6$ and the other located at $0.5f_s$.

Referring to the discussion in Section 3, based on the analysis described above, four cases: *Case A*: $f_r < 0.45 f_s$, $0 < k_w < k_{wc}$; *Case B*: $f_r < 0.45 f_s$, $k_w > k_{wc}$ and *Case C*: $f_r > 0.45 f_s$, $0 < k_w < k_c$; *Case D*: $f_r > 0.45 f_s$, $k_w > k_c$, are divided for illustrating the stability of the system with improved capacitor-current feedback active damping. Thus, according to (15), the Bode plots of $T'(z)$ for the four cases can be shown in Fig. 6*a*. As seen, without considering the $-180°$ crossing in the Nyquist frequency, in *Case B* and *Case D*, there is only one $-180°$ crossing point in the system. Thus, according to the Nyquist stability criterion, the system in *Case B and Case D* cannot be stabilized because there exist a pair of open-loop unstable poles in these two cases. In addition, since there are two and three $-180°$ crossing points in *Case A* and *Case* C, respectively, the system can be stabilized in these two cases when the following conditions satisfied

$$\begin{cases} Case\ A: \ \left| T'(z = e^{j\omega'_c T_s}) \right| < 1 \ \text{and} \ \left| T'(z = e^{j\omega'_{c2} T_s}) \right| < 1 \\ Case\ C: \ \left| T'(z = e^{j\omega'_c T_s}) \right| < 1, \ \left| T'(z = e^{j\omega'_{c2} T_s}) \right| > 1 \ \text{and} \left| T'(z = e^{j\omega'_{c3} T_s}) \right| < 1 \end{cases} \tag{19}$$

where ω'_c is the cut-off angular frequency in each case, and ω'_{c2} and ω'_{c3} is the second $-180°$ crossing angular frequency and the third $-180°$ crossing angular frequency, respectively, in each case.
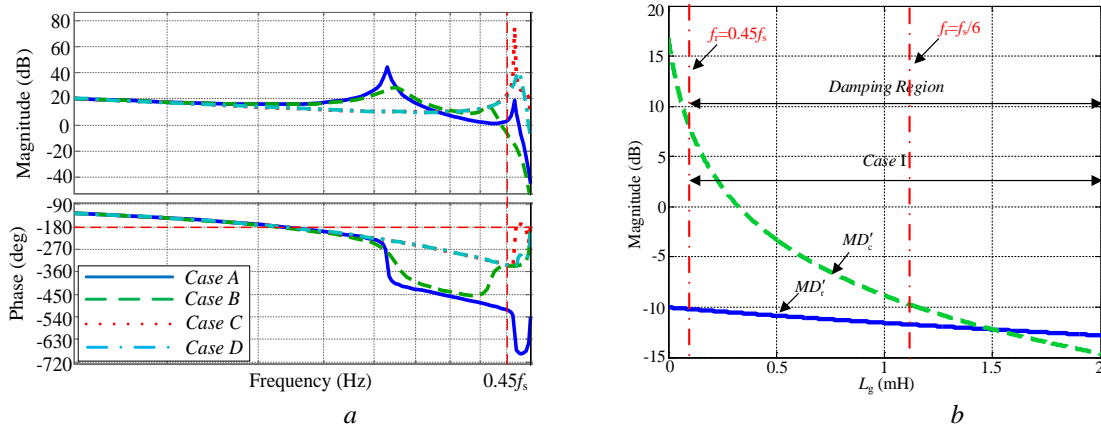
Fig. 6. *Curves of the inverter with improved capacitor-current feedback*
a. Bode plots of $T'(z)$ *for four cases*
b. Curves of MD'_r *and* MD'_c *with* L_g *varies*

4.2. Robustness against grid-impedance variation

After a detailed analysis about the damping region which is extended with the increasing of the system critical frequency in the system with improved capacitor-current feedback, the system robustness against variations in grid impedance is evaluated again for the system with improved capacitor-current feedback.

From (15), the magnitudes of the open loop system with improved capacitor-current feedback at system resonance frequency f_r and critical frequency f_c can be obtained as

$$\begin{cases} MD'_r = 20\lg\left|T'(z=e^{j\omega_r})\right|\Big\|_{G_c(z)=k_p} \\ MD'_c = 20\lg\left|T'(z=e^{j\omega_c})\right|\Big\|_{G_c(z)=k_p} \end{cases} \tag{20}$$

According to (20), the curves of MD'_r and MD'_c with the changing of grid impedance are depicted in Fig. 6*b*. As seen, compared with the curves shown in Fig. 3*a*-3*c*, the damping region of the system with improved capacitor-current feedback obviously has a larger value in Fig. 6*b*, which indicates that the robustness to grid-impedance variation has been greatly improved by the improved capacitor-current feedback.

It can be found from the above analysis that, with the increase of system critical frequency from $f_s/6$ to $0.45f_s$, the damping region is extended from $(0, f_s/6 \approx 0.17f_s)$ to $(0, 0.45f_s)$ in the system with improved capacitor-current feedback active damping. It indicates that, compared with the conventional improved capacitor-current feedback in previous paper, the stability and robustness to grid-impedance variation has been greatly expanded in the system with the capacitor-current feedback proposed in this manuscript, even in the case of the switching frequency is the same as the sampling frequency.

5. Experimental verification

A 10 kW grid-connected inverter with a LCL filter was built and tested in the lab to verify the analysis in the above section and the performance of the system with improved capacitor-current feedback active damping. The voltage and current, which are used in the control system, are sensed by voltage and current sensors, respectively. The control system is implemented in a stationary frame, thus decoupling terms are not necessary. The dual-loop control scheme is realized by a DSP control board (TMS320F28335), and synchronous sampling is adopted. To complete the experimental verification without influencing the real grid, a programmed AC source (PATS1005-PATS1900S) is used to simulate the grid-side voltage, and an external inductor is used to emulate the grid-side inductance L_g. Associated hardware was used for the protection and background routines. The main parameters of the circuit are listed in Table 1.

According to the parameters shown in Table 1 and (19), the stable boundary value of k_p in *Case* A and *Case* C can be obtained as 0.03 and 0.1, respectively. The experimental waveforms of the grid-side current i_g in *Case A and Case C* are shown in Fig. 7. As seen, when the actual resonance frequency is lower than the critical frequency and k_w is lower than k_{wc} (which is the *Case A* in Fig. 7), the waveforms of i_g have a better quality than *Case C* since a high-frequency unstable current harmonic has been introduced into the system by the open-loop unstable poles in *Case C*, which verified that the system that works within the damping region has a higher quality output current than the system that works outside the damping region.
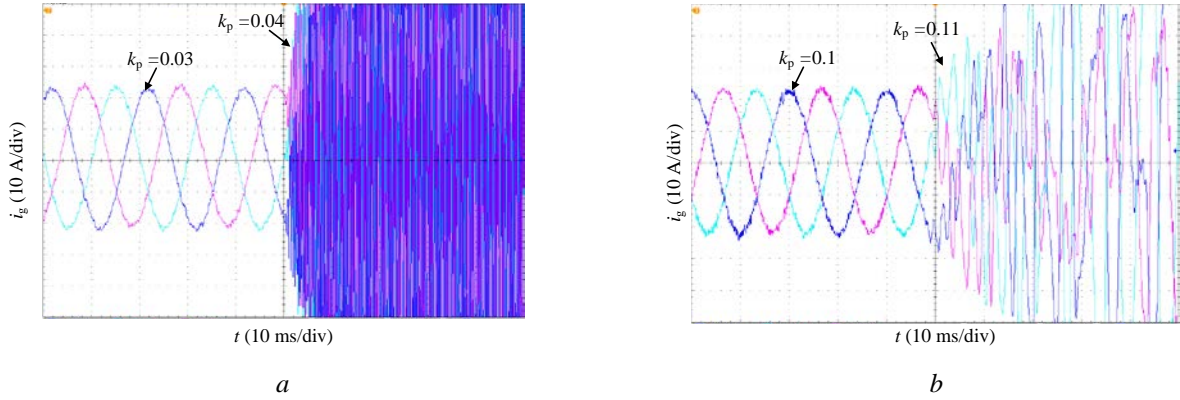

Fig. 7. *Experimental waveforms of the grid-side current i_g with k_p varying in the improved system*
a Case A: $f_r < 0.45 f_s$, $0 < k_w < k_{wc}$
b Case C: $f_r > 0.45 f_s$, $0 < k_w < k_c$

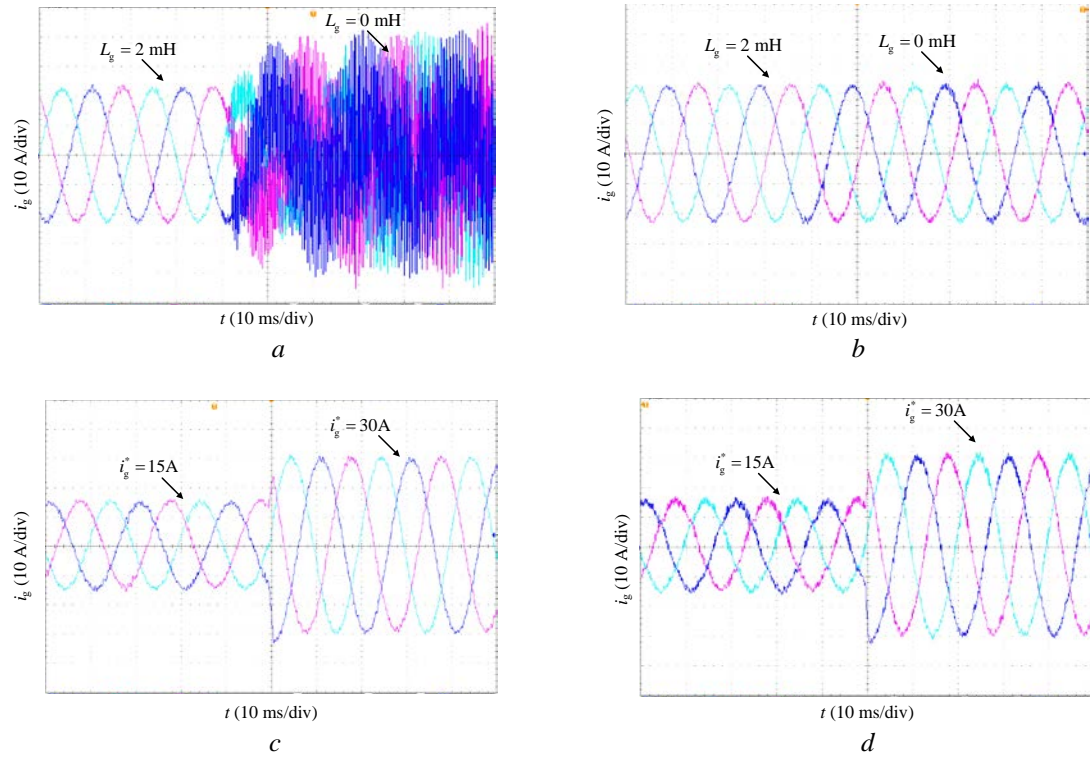**Fig. 8**. *Experimental waveforms of grid-side current i_g*
a System with the capacitor-current feedback in previous papers
b System with the improved capacitor-current feedback
c Case A: $f_r < 0.45 f_s$, $0 < k_w < k_{wc}$
d Case C: $f_r > 0.45 f_s$, $0 < k_w < k_c$

Moreover, as shown in Fig. 8, the waveforms of is become unstable when k_p is larger than its stable boundary value, which means that there exists a specific stability range for different cases and that frequency shifts arising from the grid-inductance variation may change the system case and thus make the system unstable, which verifying the discussion in the preceding sections. Therefore, in order to better cope with the system resonance frequency changes, it is desirable to extend the region of *Case* I to cover possible resonance frequencies to the greatest degree possible.

Fig. 8*a*-8*b* show the experimental waveforms of the grid-side current with grid-impedance variation in two systems, where one is the system with the improved capacitor-current feedback and the other is the system with the capacitor-current feedback that proposed in Fig. 1*b*. In order to change the system resonance frequency from 2671 Hz ($< f_s/6$) to 7293 Hz ($> f_s/6$, $< 0.45 f_s$) with the grid-impedance decreasing from 2 mH to 0 mH, $L_2 = 0.2$ mH is used. As shown in Fig. 8*a*-8*b*, with the decrease of the grid inductance, the grid-side current in Fig. 8*a* becomes unstable when the system resonance frequency is higher than the system critical frequency ($f_s/6$). However, compared with the grid-side current in Fig. 8*a*, the grid-side current in

16

Fig. 8*b* can always be stable and has a good quality in a large frequency range. This is thanks to the fact that critical frequency in this system been extended to $0.45f_s$ which gives the system a wider stable operation region $(0, 0.45f_s)$ and thus a higher robustness against grid-impedance variation is achieved in the system with the improved capacitor-current feedback.

To show the dynamic performance of the system with the improved active damping loop, the transient experimental waveforms of i_g, where the command current i_g^* is step-changed from 15 to 30 A (peak value), for *Case A and Case C* are shown in Fig. 8*c*-8*d*. As seen, the system shows a satisfactory damping performance to dampen the dynamic oscillation, which resulted by good damping, with a rise time of 1ms.

The experimental results presented above shows that the improved active damping loop can obtain a better damping performance and retains a satisfactory dynamic performance at the same time.

6. Conclusion

This paper presents a study of the effects of damping region on digitally controlled LCL-type grid-connected system with capacitor-current feedback. It found that, the system that works in the damping region can obtain a better robustness against grid impedance variation. However, the damping region is considerably small in the digitally controlled system because the influence of digital time delay results in high values of inductance and capacitance of LCL filter to ensure that the system works within the system damping region. To address this issue for the case when the ratio between the sampling frequency to the switching frequency is lower than 2, an improved capacitor-current feedback method was proposed to increase the system critical frequency to $0.45f_s$, which can cover almost all possible resonance frequencies under the case the ratio between the sampling frequency to the switching frequency is lower than 2 because of the change in the system sampling mode. With this method, the LCL-type grid-connected inverter can obtain satisfactory steady-state and transient-state performance while achieving a wider active damping region, thereby increasing the stability of the digitally controlled system and the robustness of system to grid-impedance variation with a lower value of inductance and capacitance of LCL filter, no matter how the sampling mode changes.

7. Acknowledgments

8. Appendix

The coefficients in (18) are listed as follows:

$b_1=\cos(6\omega T_s)+(a_4-1)\cos(5\omega T_s)+(a_3-a_4)\cos(4\omega T_s)+(a_2-a_3)\cos(3\omega T_s)+(a_1-a_2)\cos(2\omega T_s)-a_1\cos(\omega T_s),$

$b_2=\sin(6\omega T_s)+(a_4-1)\sin(5\omega T_s)+(a_3-a_4)\sin(4\omega T_s)+(a_2-a_3)\sin(3\omega T_s)+(a_1-a_2)\sin(2\omega T_s)-a_1\sin(\omega T_s),$

$d_1=(\omega_r T_s c_1-c_3\sin(\omega_r T_s)),\ d_2=(\omega_r T_s c_2-c_4\sin(\omega_r T_s));$

$c_1=\cos(4\omega T_s)+a_4\cos(3\omega T_s)+(a_3-\delta)\cos(2\omega T_s)+(a_2+\delta)\cos(\omega T_s),$

$c_2=\sin(4\omega T_s)+a_44\sin(3\omega T_s)+(a_3-\delta)\sin(2\omega T_s)+(a_2+\delta)\sin(\omega T_s),$

$c_3=\cos(4\omega T_s)+(2\gamma-2)\cos(3\omega T_s)+(1+\gamma^2-4\gamma)\cos(2\omega T_s)+(2\gamma-2\gamma^2)\cos(\omega T_s)+\gamma^2,$

$c_4=\sin(4\omega T_s)+(2\gamma-2)\sin(3\omega T_s)+(1+\gamma^2-4\gamma)\sin(2\omega T_s)+(2\gamma-2\gamma^2)\sin(\omega T_s);$

$a_1=\gamma^2,\ a_2=2\gamma-2\gamma^2\cos(\omega_r T_s)-\delta,\ \ a_3=1-4\gamma\cos(\omega_r T_s)+\gamma^2+\delta,\ \ a_4=2\gamma-2\cos(\omega_r T_s);\ \ \delta=k_{pwm}k_w\sin(\omega_r T_s)/\omega_r L_1;\ \gamma=0.98.$

9. References

[1] Tang Y., Loh P. C., Wang P., Choo F. H., and Gao F.: 'Exploring inherent damping characteristic of *LCL*-filters for three-phase grid-connected voltage source inverters', *IEEE Trans. Power Electron.*, 2012, **27**, (3), pp. 1433–1443

[2] Busada C. A., Jorge S. G., and Solsona J. A.: 'Full-state feedback equivalent controller for active damping in *LCL* filtered grid connected inverters using a reduced number of sensors', *IEEE Trans. Ind. Electron.*, 2015, **62**, (10), pp. 5993–6002

[3] Chen C., Xiong J., Wan Z. Q., Lei J., and Zhang K.: 'A time delay compensation method based on area quvialence for active damping of an LCL-type converter', *IEEE Trans. Power Electron.*, 2017, **32**, (1), pp. 762–772

[4] Bao C., Ruan X., Wang X., Li W., Pan D., and Weng K.: 'Design of injected grid current regulator and capacitor-current-feedback active-damping for *LCL*-type grid-connected inverter', in *Proc. IEEE ECCE*, 2012, pp. 579–586

[5] Wang J., Yan J. D., Jiang L., and Zou J.: 'Delay-dependent stability of single-loop controlled grid-connected inverters with *LCL* filters', *IEEE Trans. Power Electron.*, 2016, **31**, (1), pp. 743–757

[6] Mohamed Y. A. I.: 'Mitigation of dynamic, unbalanced, and harmonic voltage disturbances using grid-connected inverters with *LCL* filte', *IEEE Trans. Ind. Electron.*, 2011, **58**, (9), pp. 3914–3924

[7] Zhang X., J. W. Spencer, and J. M. Guerrero: 'Small-signal modeling of digitally controlled grid-connected inverters with *LCL* filters', *IEEE Trans. Ind. Electron.*, 2013, **60**, (9), pp. 3752–3765

[8] Pan D., Ruan X., Bao C., Li W., and Wang X.: 'Capacitor-current-feedback active damping with reduced computation delay for improving robustness of *LCL*-type grid-connected inverter', *IEEE Trans. Power Electron.*, 2014, **29**, (7), pp. 3414–3427

[9] Wagner M., Barth T., Alvarez R., Ditmanson C., and Bernet S.: 'Discrete time active damping of *LCL*-resonance by proportional capacitor current feedback', *IEEE Trans. Ind. Appl.*, 2014, **50**, (6), pp. 3911–3920

[10] Li X. Q., Wu X. J., Geng Y. W., Yuan X. B., Xia C. Y., and Zhang X.: 'Wide damping region for *LCL*-type grid-connected inverter with an improved capacitor-current-feedback methos', *IEEE Trans. Power Electron.*, 2015, **30**, (9), pp. 5247–5259

[11] Li R., Liu B., Duan S., Yin J., and Jiang X.: 'Analysis of delay effects in single-loop controlled grid-connected inverter with *LCL* filter in *Proc. IEEE Appl. Power Electron*', *Conference*, pp. 329–333, 2013

[12] Guo X. Q. and Guerrero J. M.: 'General unified integral controller with zero steady-state error for single-phase grid-connected inverters', *IEEE Trans. Smart Grids*, 2016, **7**, (1), pp. 74–83

[13] Li W., Ruan X., Pan D., and Wang X.: 'Full-feedforward schemes of grid voltages for a three-phase *LCL*-type grid-connected inverter', *IEEE Trans. Ind. Electron.*, 2013, **60**, (6), pp. 2237–2250

[14] Liu Y., Wu W. M., He Y. B., Lin Z., Blaabjerg F., and Chung H. S.-H.: 'An efficient and robust hybrid damper for *LCL*- or *LLCL*-based grid-tied inverter with strong grid-side harmonic voltage effect injection', *IEEE Trans. Ind. Electron.*, 2016, **63**, (2), pp. 926–936

[15] Liu J. H., Zhou L., Yu X. R., Li B., and Zheng C.: '*LCL* filter design and performance analysis for grid-interconnected systems', *IET Power Electron.*, 2017, **10**, (2), pp. 232–239

[16] Dannehl J., Fuchs F. W., Hansen S., and Thøgersen P. B.: 'Investigation of active damping approaches for PI-based current control of grid-connected pulse width modulation converters with *LCL* filters', *IEEE Trans. Ind. Appl.*, 2010, **46**, (4), pp. 1509–1517

[17] Astrom K. J., and Wittenmark B., *Computer Controlled Systems*. Englewood Cliffs, NJ: Prentice-Hall, 1990, pp. 209-243

[18] Orellana M., and GriñóR.: 'On the stability of discrete-time active damping methods for VSI converters with a *LCL* input filter', in *Proc. IEEE IECON,* 2012, pp. 2378–2383

[19] Miskovic V., Blasko V., Jahns T. M., Smith A. H. C., and Romenesko C.: 'Observer based active damping *LCL* resonance in grid-connected voltage source converters', *IEEE Trans. Ind. Appl.*, 2010, **50**, (6), pp. 3977–3985

[20] Chen C., Xiong J., Wan Z. Q., Lei J., and Zhang K.: 'Time delay compensation method based on area equivalence for active damping of *LCL*-type converter', *IEEE Trans. Power Electron.*, 32, no. 1, 762–772. doi: 10.1109/TPEL.2016.2531183

[21] Parker S. G., McGrath B. P., and Holmes D. G.: 'Regions of active damping control for *LCL* filters', *IEEE Trans. Ind. Appl.*, 2014, **50**, (1), pp. 424–432

[22] Xin Z., Wang X. F., Loh P. C., and Blaabjerg F.: 'Grid-current feedback control for *LCL*-filtered grid converters with enhanced stability', *IEEE Trans. Power Electron.*, 1–1. doi: 10.1109/TPEL.2016.2580543.

[23] Wang X., Blaabjerg F., and Loh P. C.: 'Virtual RC damping of *LCL* filtered voltage source converters with extended selective harmonic compensation', *IEEE Trans. Power Electron.*, 2015, **30**, (9), pp. 4726–4737

[24] Taylor F., *Digital Filters: Principles and Applications with MATLAB*. New York, NY, USA: IEEE Press, 2012